AGU PUBLICATIONS

JGR

Journal of Geophysical Research: Space Physics

RESEARCH ARTICLE

10.1002/2014JA020243

On the day-to-day variation of the equatorial electrojet during quiet periods

Y. Yamazaki[1,2], A. D. Richmond[2], A. Maute[2], H.-L. Liu[2], N. Pedatella[3], and F. Sassi[4]

[1]Department of Physics, University of Lancaster , Lancaster, UK, [2]High Altitude Observatory, National Center for Atmospheric Research, Boulder, Colorado, USA, [3]COSMIC Program Office, University Corporation for Atmospheric Research, Boulder, Colorado, USA, [4]Space Science Division, Naval Research Laboratory, Washington, District of Columbia, USA

Key Points:
- Day-to-day variation of the equatorial electrojet (EEJ) is simulated
- A current system associated with EEJ variability is revealed
- The EEJ variability is dominated by equatorial zonal wind at 110 km

Correspondence to:
Y. Yamazaki,
y.yamazaki@lancaster.ac.uk

Citation:
Yamazaki, Y., A. D. Richmond, A. Maute, H.-L. Liu, N. Pedatella, and F. Sassi (2014), On the day-to-day variation of the equatorial electrojet during quiet periods, *J. Geophys. Res. Space Physics*, *119*, 6966–6980, doi:10.1002/2014JA020243.

Received 2 JUN 2014
Accepted 7 AUG 2014
Accepted article online 11 AUG 2014
Published online 28 AUG 2014

Abstract It has been known for a long time that the equatorial electrojet varies from day to day even when solar and geomagnetic activities are very low. The quiet time day-to-day variation is considered to be due to irregular variability of the neutral wind, but little is known about how variable winds drive the electrojet variability. We employ a numerical model introduced by Liu et al. (2013), which takes into account weather changes in the lower atmosphere and thus can reproduce ionospheric variability due to forcing from below. The simulation is run for May and June 2009. Constant solar and magnetospheric energy inputs are used so that day-to-day changes will arise only from lower atmospheric forcing. The simulated electrojet current shows day-to-day variability of ±25%, which produces day-to-day variations in ground level geomagnetic perturbations near the magnetic equator. The current system associated with the day-to-day variation of the equatorial electrojet is traced based on a covariance analysis. The current pattern reveals return flow at both sides of the electrojet, in agreement with those inferred from ground-based magnetometer data in previous studies. The day-to-day variation in the electrojet current is compared with those in the neutral wind at various altitudes, latitudes, and longitudes. It is found that the electrojet variability is dominated by the zonal wind at 100–120 km altitudes near the magnetic equator. These results suggest that the response of the zonal polarization electric field to variable zonal winds is the main source of the day-to-day variation of the equatorial electrojet during quiet periods.

1. Introduction

The ionosphere is electrically conducting due to the presence of free electrons and ions and thus allows electric currents to flow. At middle and low geomagnetic latitudes (below 60°), ionospheric currents are mainly driven through the ionospheric wind dynamo mechanism [*Richmond*, 1995a]. The neutral wind in the dynamo region (approximately 90–150 km) generates an electromotive force $\mathbf{v} \times \mathbf{B}_0$ as it moves the electrically conducting air across the geomagnetic field, where $\mathbf{v}$ is the wind velocity and $\mathbf{B}_0$ is the Earth's main magnetic field. Generally, the wind-induced currents are not divergence free, and thus, a polarization electrostatic field is set up so as to maintain closure of the total current. The ionospheric wind dynamo currents are responsible for the daily variation of the geomagnetic field on the ground during magnetically quiet periods, which is often referred to as solar quiet (*Sq*) variation [*Matsushita*, 1967; *Campbell*, 2003]. One of the most remarkable features of the ionospheric wind dynamo current system is an enhanced eastward current flow along the magnetic equator, which is commonly known as the equatorial electrojet [*Forbes*, 1981; *Rastogi*, 1989]. At the magnetic equator, where geomagnetic field lines are horizontal, a strong vertical polarization electric field can be established, which effectively increases the zonal ionospheric conductivity. A manifestation of the equatorial electrojet is a large *Sq* variation in the horizontal or magnetic northward (*H*) component of the geomagnetic field near the magnetic equator. The equatorial electrojet has also been studied using in situ rocket measurements [*Onwumechili*, 1997, and references therein] and satellite data [e.g., *Lühr et al.*, 2004; *Alken and Maus*, 2007]. Studies of the equatorial electrojet have provided significant insight into equatorial electrodynamic processes, which play an important role in low-latitude space weather [*Stening*, 2003].

It has been known from studies of *Sq* variations that ionospheric wind dynamo currents vary significantly from day to day [*Chapman and Bartels*, 1940; *Hasegawa*, 1960; *Briggs*, 1984; *Takeda*, 1984]. The day-to-day variation is persistent even when changes in solar and geomagnetic activities are apparently absent, and therefore, irregular variability in the neutral wind is considered to be the main source. *Miyahara and Ooishi*

[1997] studied the feasibility of this idea by means of a numerical simulation. They computed ionospheric wind dynamo currents using a thin-shell electrodynamics model, with wind forcing including upward propagating tides and other large-scale waves from the lower atmosphere. They found that the waves from below the ionosphere can induce day-to-day variations in the dynamo currents. More recent work, involving three-dimensional electrodynamics models and more realistic driving winds, has also demonstrated a significant contribution of lower atmospheric forcing to the day-to-day variation of the ionospheric wind dynamo [*Kawano-Sasaki and Miyahara*, 2008; *Jin et al.*, 2011; *Liu et al.*, 2013; *Fang et al.*, 2013]. However, it is not well understood how irregular variability in the neutral wind drives the variability in the current. In the present study, we use the model introduced by *Liu et al.* [2013] to study the electrojet variability and its relation to the neutral wind in order to elucidate the driving mechanism of the day-to-day variation of the equatorial electrojet during quiet periods.

2. Model and Data

2.1. TIME-GCM

We use the thermosphere-ionosphere-mesosphere electrodynamics general circulation model (TIME-GCM) developed at National Center for Atmospheric Research [*Roble and Ridley*, 1994]. The TIME-GCM is a three-dimensional time-dependent model of the Earth's middle and upper atmosphere. The model incorporates mutual coupling between the thermosphere and ionosphere with a self-consistent electrodynamic scheme [*Richmond et al.*, 1992]. The horizontal resolution is 2.5° in geographic latitude and longitude. For electrodynamics calculations, a finer latitudinal grid (~0.5° near the magnetic equator) is used to resolve the equatorial electrojet. The model uses constant pressure surfaces as the vertical coordinate. The pressure interfaces are defined as $Z = \ln(P0/P)$, where P is pressure and $P0 = 5 \times 10^{-7}$ hPa. The upper and lower boundaries are at $Z = 7$ (4.6×10^{-10} hPa) and $Z = -17$ (12 hPa), respectively, which correspond to 480 and 30 km for solar minimum conditions. The vertical resolution is a quarter-scale height.

The electrodynamics of the TIME-GCM is calculated in the Magnetic Apex coordinate system [*Richmond*, 1995b] using the International Geomagnetic Reference Field [*Finlay et al.*, 2010]. Geomagnetic field lines are assumed to be equipotential, and current may flow between hemispheres along these lines at middle and low latitudes. The TIME-GCM artificially increases the electron-neutral collision frequency by a factor of 4 in order to reduce the current strength in the bottom side of the electrojet. This ad hoc modulation of the electron-neutral collision frequency is known to improve agreement between models and observations of the equatorial electrojet [*Gagnepain et al.*, 1977] but has little effect on global-scale electric fields and currents. It approximately simulates the effects of plasma irregularities on the current but does not account for the possibility that these effects might depend on the current strength. Geomagnetic daily variations at ground level are computed from height-integrated horizontal currents as described by *Richmond and Maute* [2014]. The TIME-GCM uses a very simple model of the Earth electrical conductivity, which assumes the existence of a perfectly conducting layer at 600 km depth where the vertical magnetic perturbations vanish.

Solar EUV and FUV spectral fluxes in the TIME-GCM can be specified using the EUVAC model [*Richards et al.*, 1994] with an input of solar radiation index $F_{10.7}$. We use the EUVAC model, but the soft X-ray fluxes (wavelengths between 8 and 70 Å) are increased by a factor of 4.4, which will achieve reasonably accurate daytime ionospheric conductivities with little impact on the F region plasma [*Fang et al.*, 2008a]. All the simulations are run with a constant solar energy input under a solar minimum condition; $F_{10.7} = 70$ solar flux unit (sfu). We also assume a constant magnetospheric energy input. The hemispheric power and cross-polar cap potential are set to 18 GW and 31 kV, respectively, which is representative of a quiet geomagnetic condition with $Kp = 1.0$. Consequently, solar and geomagnetic activities do not cause the ionospheric day-to-day variability in the model. The day-to-day variability in the model arises solely from lower atmospheric forcing that is described in the following paragraphs.

2.2. WACCM-X/MERRA/NOGAPS-ALPHA

Forcing from the lower atmosphere is introduced by constraining the lower part (below 95 km) of the TIME-GCM by the extended version of the Whole Atmosphere Community Climate Model (WACCM-X) [*Liu et al.*, 2010a; *Liu*, 2014] with specified dynamical fields from the Modern Era Retrospective Analysis for Research and Applications (MERRA) [*Rienecker et al.*, 2011] and U.S. Navy's Operational Global Atmospheric Prediction System Advanced Level Physics High Altitude (NOGAPS-ALPHA) [*Hoppel et al.*, 2008; *Eckermann*

et al., 2009] data assimilation products. See *Sassi et al.* [2013] for the method of specifying the WACCM-X dynamical fields using MERRA and NOGAPS-ALPHA data. We refer to this particular configuration of the WACCM-X as WACCM-X/MERRA/NOGAPS-ALPHA. *Sassi et al.* [2013], examining the WACCM-X/MERRA/NOGAPS-ALPHA results for the January 2009 stratospheric sudden warming event, demonstrated that the model properly represents a broad spectrum of atmospheric waves, from tidal waves to Rossby and Rossby-gravity normal modes, and ultrafast Kelvin waves, as well as the mean circulation.

The TIME-GCM solutions are nudged toward the WACCM-X/MERRA/NOGAPS-ALPHA predictions for the heights from the TIME-GCM lower boundary (~30 km) to 95 km, in the way described by *Liu et al.* [2013]. The nudging is achieved by applying a tendency to the neutral wind and temperature in the TIME-GCM. The tendency acts to force the TIME-GCM neutral wind and temperature toward the values obtained from the WACCM-X/MERRA/NOGAPS-ALPHA. The tendency maximizes at the lower boundary of the TIME-GCM, where the TIME-GCM neutral wind and temperature fields are overwritten by the corresponding fields from the WACCM-X/MERRA/NOGAPS-ALPHA, and is gradually reduced to zero at 95 km.

The TIME-GCM nudged by the WACCM-X/MERRA/NOGAPS-ALPHA is run from 1 May through 30 June 2009, when geomagnetic activity was particularly low. The following parameters are output every hour starting from 0030 universal time (UT) on 3 May 2009: magnetic eastward current density, eastward and northward neutral winds, and *H* component *Sq* variations at ground level.

2.3. Geomagnetic Data

Ground-based magnetometer data at Tirunelveli (8.7°N, 77.8°E) and Huancayo (12.1°S, 284.7°E) are also analyzed for a comparison with the model results. Both stations are located near the magnetic equator and thus under the effect of the equatorial electrojet. The hourly data were provided by the World Data Center for Geomagnetism (Edinburgh). The *Dst* index was subtracted from the *H* component in order to minimize the effect of magnetospheric currents. The average of the five nighttime hourly values starting from 0000 local time was used as the zero level of the *Sq* variation, which is justified as the ionospheric conductivity at dynamo region heights becomes much smaller during nighttime than daytime.

3. Results and Discussion

3.1. Neutral Wind

Figures 1a and 1b show the average amplitude of the migrating diurnal and semidiurnal tides, respectively, in the TIME-GCM nudged by the WACCM-X/MERRA/NOGAPS-ALPHA. Using the zonal wind for May and June 2009, the tidal components were extracted on the basis of least squares fitting [*Wu et al.*, 2006]. Satellite-borne magnetometer measurements have shown that those tidal components are dominant in the electrojet spectra [*Lühr and Manoj*, 2013].

The migrating diurnal tide has a peak in the lower thermosphere (about 95 km) at −20° latitude. The height of the peak amplitude is where the tidal waves from below, which grow with altitude, are damped due to strong dissipation by eddy diffusion. Above 110 km, the amplitude of the migrating diurnal tide starts to increase again with altitude due to in situ forcing by solar ultraviolet heating. The diurnal tide locally excited in the thermosphere is considered to be the primary driver of ionospheric wind dynamo currents [*Richmond et al.*, 1976; *Richmond and Roble*, 1987], and it accounts for about half of the equatorial electrojet current [*Yamazaki et al.*, 2014]. In our simulation, solar heating is kept constant so that the thermosherically generated diurnal tide will make little contribution to the equatorial electrojet variability.

The migrating semidiurnal tide peaks at about 120 km at ±60° latitudes. The upward propagating migrating semidiurnal tide can reach higher altitudes compared to the diurnal tide, because it has a longer vertical wavelength and faster vertical group velocity [*Yamazaki and Richmond*, 2013]. The migrating semidiurnal tide due to in situ forcing in the thermosphere is much weaker than the diurnal tide [*Hagan et al.*, 2001].

Comparisons with previously published observations [*Khattatov et al.*, 1997; *Wu et al.*, 2008; *Xu et al.*, 2009] suggest that the migrating diurnal tide from the lower atmosphere is too weak in the model, as the observations show the peak amplitudes of the migrating diurnal tide to be 20–40 m/s in the mesosphere and lower thermosphere (MLT) region for this season. Studies have shown that the WACCM tends to underestimate tides in the MLT region. For example, *Davis et al.* [2013], comparing WACCM results with tropical wind observations in the MLT region, found that the diurnal tide in the WACCM is too small. The underestimation of tides in the WACCM could arise from various reasons. *Liu et al.* [2010a] pointed out that the vertical

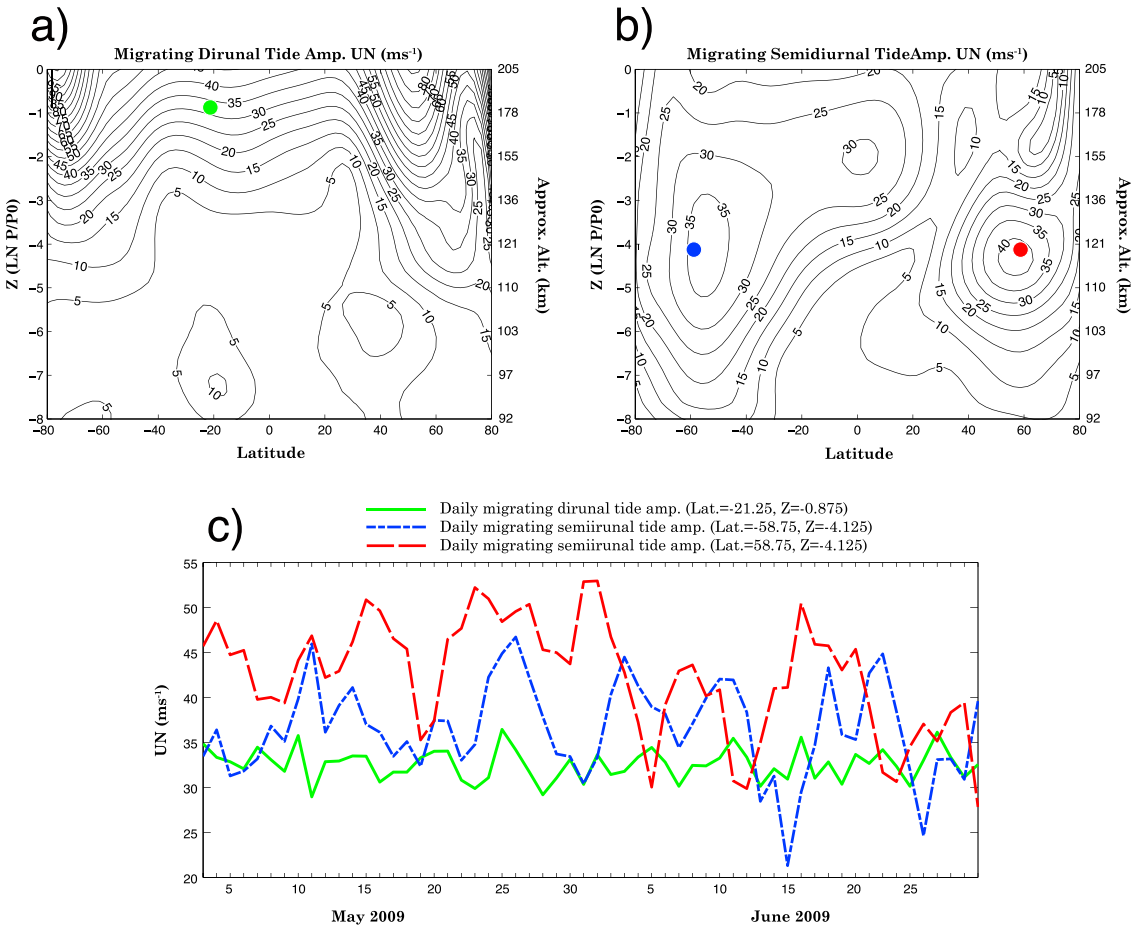

Figure 1. Height versus latitude distributions of the average amplitude for (a) migrating diurnal tide and (b) migrating semidiurnal tide for the zonal wind in the TIME-GCM nudged by the WACCM-X/MERRA/NOGAPS-ALPHA for May and June 2009. (c) Daily amplitudes of the migrating diurnal tide near −20° at ∼180 km (green) , the migrating semidiurnal tide near −60° at ∼120 km (blue), and the migrating semidiurnal tide near 60° at ∼120 km (red).

resolution of the WACCM may not be sufficient in the MLT region to fully resolve the migrating diurnal tide. *Pedatella et al.* [2014a] found that gravity wave forcing, which affects the vertical propagation of tides and tends to dampen them, is rather strong in the WACCM compared with other whole atmosphere models. Despite the probable underestimation of migrating diurnal tidal forcing from below, the model electrojet current will be shown to be reasonably strong on average. As mentioned earlier, the migrating diurnal tide that is important for the background equatorial electrojet strength is those locally generated in the thermosphere, not those propagating from the lower atmosphere. However, it is still possible that weak migrating diurnal tidal forcing from the lower atmosphere leads to the underestimation of dynamo region wind variability and thus electrojet variability.

Figure 1c illustrates day-to-day changes in the tides. The daily amplitude of the migrating semidiurnal tide shows significant variability around its peak latitude and height (blue and red). It is interesting to note that the amplitude at the southern peak does not correlate with that at the northern peak. Although the migrating semidiurnal tide is a global-scale wave, its symmetric and antisymmetric components vary from day to day, which causes the temporal correlation at distant two locations to be small. The migrating diurnal tide in the thermosphere (approximately 180 km) shows a relatively small day-to-day variation (green) because the migrating diurnal tide at this altitude is mainly driven locally by solar ultraviolet heating, which is constant in our simulation. The large day-to-day variations in the semidiurnal tide can result from various sources. First, weather changes in the lower atmosphere can affect the distribution of heating sources for tides, such as H_2O and O_3. Second, tidal waves can be modulated through nonlinear interaction between the tide and other waves (or the tide itself) [*Teitelbaum et al.*, 1989; *Teitelbaum and Vial*, 1991; *Liu et al.*, 2010b]. Third, dissipating tides and other waves drive changes in the background atmosphere, which affect upward

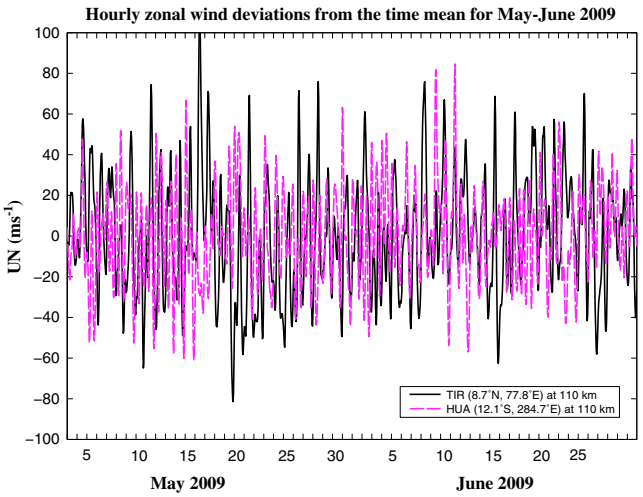

Figure 2. Simulated hourly zonal wind speed at Tirunelveli (black) and at Huancayo (magenta) at 110 km for May and June 2009. Plotted are deviations from the time average.

propagation of tidal waves from the lower atmosphere to the upper atmosphere [*Miyahara*, 1978; *Miyahara and Forbes*, 1991; *Stening et al.*, 1997; *Chang et al.*, 2011]. Lastly, the resonance property of the atmosphere changes with time as the background atmosphere varies, which can cause the amplification of atmospheric waves with certain periods [*Forbes and Zhang*, 2012].

Although we have shown only migrating diurnal and semidiurnal tides, other tides and large-scale waves from the lower atmosphere are also present at dynamo region heights, and they also change in a complex manner through the mechanisms mentioned above. As a result, the temporal variation in the wind speed at any fixed location (altitude, latitude, and longitude) is highly irregular. An example is given in Figure 2, where hourly values of the zonal wind speed are plotted for Tirunelveli (8.7°N, 77.8°E) and Huancayo (12.1°S, 284.7°E) at 110 km for May and June 2009. We will examine, in section 3.4, the relationship between irregular variability of the wind and equatorial electrojet current.

The lunar tide is not included in the models we use. According to observations, the peak amplitude of the migrating semidiurnal lunar tide in the wind is usually about 10–15 m s^{-1} in the MLT region [*Zhang and Forbes*, 2013; *Forbes et al.*, 2013]. It is known that the effect of the lunar tide modulates the equatorial electrojet [*Rastogi and Trivedi*, 1970; *Rastogi*, 1974]. The lunar tide plays a particularly important role in driving electrodynamic effects during stratospheric sudden warmings [*Pedatella et al.*, 2012, 2014b], but for other periods, the contribution to the equatorial electrojet is much smaller, about a tenth that of solar tides [*Yamazaki et al.*, 2011]. Therefore, it is assumed that the neglect of the lunar tide does not significantly affect the results presented in this study.

3.2. *Sq* Variations at Tirunelveli and Huancayo

Figures 3a and 3b show the average of the *H* component *Sq* variation at Tirunelveli and Huancayo, respectively, for May and June 2009. Both stations are located near the magnetic equator, and thus, the *Sq* variations mainly reflect changes in the equatorial electrojet intensity above. In the figures, the blue lines indicate observations, and the red lines indicate the results from the TIME-GCM nudged by the WACCM-X/MERRA/NOGAPS-ALPHA. Both observed and simulated *Sq*(*H*) reach maximum around the noon, indicative of the eastward current. The daily range of the *Sq*(*H*) is greater at Huancayo than Tirunelveli. This is owing to the weaker background geomagnetic field at Huancayo, which leads to larger ionospheric conductivities [*Shinbori et al.*, 2010]. The *Sq* variations derived using only days when the maximum *Kp* is equal to or less than 2.0 yielded almost identical results.

Figures 3c and 3d show the difference between observed and simulated *Sq*(*H*) at Tirunelveli and Huancayo, respectively. The green lines indicate differences on individual days, and the black lines indicate their average. At Tirunelveli, the model tends to underestimate *Sq*(*H*) during the morning while it overestimates *Sq*(*H*) during the afternoon. Such a systematic discrepancy may result from inaccuracy in the phase of semidiurnal tides in the model. The errors at Huancayo are more random.

Figure 4 depicts day-to-day changes in (a) geomagnetic activity, (b) solar radiation flux, (c) *Sq*(*H*) at Tirunelveli, and (d) *Sq*(*H*) at Huancayo, from 3 May to 30 June 2009. Geomagnetic activity was very low during this period. There were a few minor disturbances with the daily maximum *Kp* $\geq$4.0, but none of them caused a geomagnetic storm. Solar activity was also very low with the average $F_{10.7}$ index 71.5 sfu and stayed nearly constant. Both observed (blue) and simulated (red) *Sq* variations show day-to-day variability. The counter electrojet at Huancayo on 7 May, 25 June, and 29 June, which can be seen as negative values

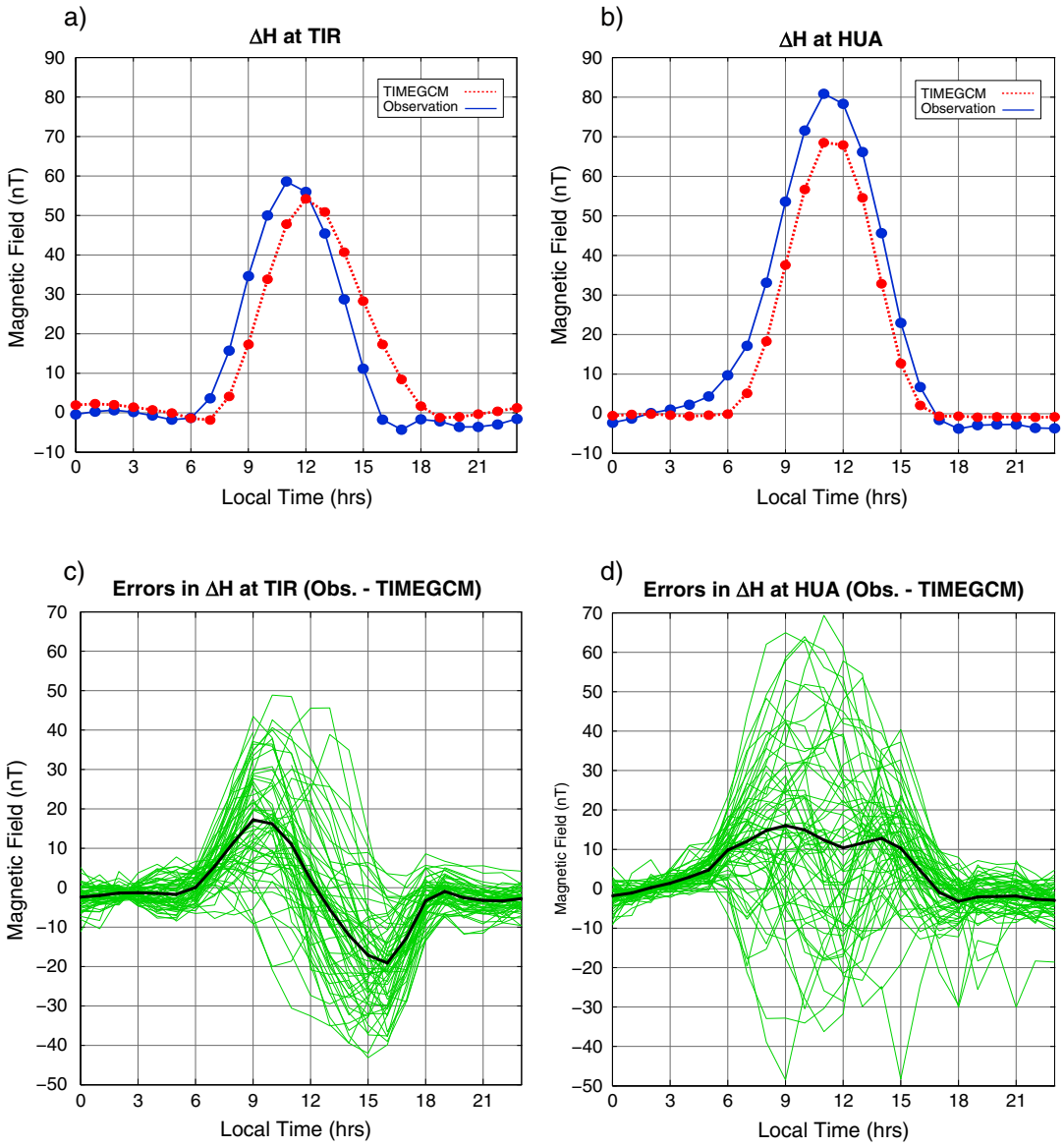

Figure 3. Average daily variations of the *H* component geomagnetic field at (a) Tirunelveli and at (b) Huancayo, for May and June 2009. The blue solid lines denote observations, and the red dashed lines denote the simulation results from the TIME-GCM nudged by the WACCM-X/MERRA/NOGAPS-ALPHA. (c and d) Differences between observed and simulated *Sq*(*H*) are also shown, where the thin green lines indicate the results on individual days and the thick black lines indicate their average.

in *Sq*(*H*) about −25 nT, seems to be correlated with geomagnetic disturbances. Previous studies found that geomagnetic disturbances can cause the counter electrojet through the disturbance dynamo mechanism [*Blanc and Richmond*, 1980; *Le Huy and Amory-Mazaudier*, 2005] and the penetration of the high-latitude electric field into equatorial latitudes [*Kikuchi et al.*, 2008]. Interestingly, the counter electrojet associated with geomagnetic disturbances is not as apparent at Tirunelveli. Since the simulation was run under a constant geomagnetic activity condition, the model does not reproduce this type of counter electrojet.

Observations show the counter electrojet (~20 nT) even during quiet days. According to previous studies, the quiet day counter electrojet event is often accompanied by abnormal *Sq* variations at middle and low latitudes, which is believed to be caused by changes in the tidal wind composition in the dynamo region [*Stening*, 1977; *Gurubaran*, 2002; *Yamazaki et al.*, 2012]. Our simulation results also show the quiet day counter electrojet (~5 nT), but the magnitude is much smaller than observations. The underestimation of the quiet day counter electrojet may result from imperfect description of the tidal spectrum in the model.

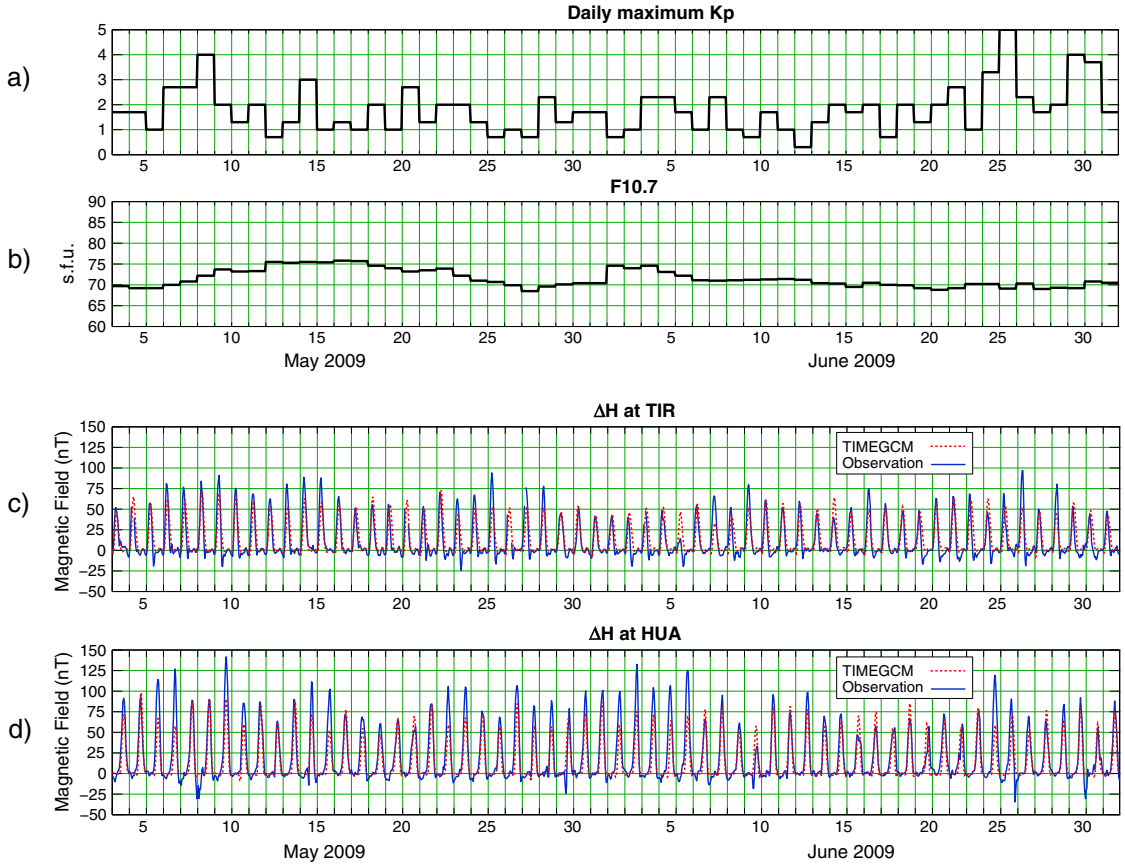

Figure 4. (a) Daily maximum *Kp* values for May and June 2009. (b) Daily values for the solar activity index $F_{10.7}$. (c) Daily variations of the *H* component geomagnetic field at Tirunelveli. (d) Daily variations of the *H* component geomagnetic field at Huancayo. Note that the TIME-GCM is run using constant *Kp* and $F_{10.7}$ values.

Next, we examine the day-to-day variation in the daily range of *Sq*(*H*). Table 1 shows various parameters and their interrelationship derived from the analysis. We found no significant correlation between the day-to-day variations at Tirunelveli and Huancayo, in either observation or simulation results. *Schlapp* [1968] showed that the correlation of the daily range of *Sq*(*H*) decreases with increasing distance between two stations, reaching 0.5 for separations of about 40° in longitude and 15° in latitude. The longitude separation between Tirunelveli and Huancayo is 153.1°. The ratio of the standard deviation to the average represents the magnitude of the day-to-day variation, which is about 25% for the observations and 15% for the model results. The correlation between the observed and simulated day-to-day variations is about 0.35 for quiet days at both locations. This indicates that the model reproduces at least a part of actual variability, not just random fluctuations.

As indicated by the large counter electrojet at Huancayo during moderately disturbed days, the observations are not completely free from the influence of geomagnetic activity despite the fact that the overall geomagnetic activity level is very low during the period investigated. Selecting the quiet days ($Kp \leq 2.0$) is not sufficient to completely remove the effect of geomagnetic activity changes. For instance, the influence of the disturbance wind can last for many days after geomagnetic activity ceases owing to the inertia of the neutral air [*Huang et al.*, 2005]. The effect of lower atmospheric forcing and geomagnetic activity on the day-to-day *Sq* variability can be separately evaluated only when the model including realistic forcing of both kinds reproduces the observations reasonably well. Lately, *Marsal et al.* [2012] used field-aligned currents measured by the Active Magnetosphere and Planetary Electrodynamics Response Experiment satellite to incorporate realistic variability of high-latitude electrodynamics in their model. Inclusion of such a realistic high-latitude forcing scheme is beyond the scope of this study, as we focus on the driving mechanism of the day-to-day electrojet variability due to variable winds.

Table 1. The Daily Range of $Sq(H)$, Which is Denoted as R_j^i[a]

		Correlation Coefficient
R^{TIR}_{Obs} versus R^{HUA}_{Obs}		0.1
R^{TIR}_{Mod} versus R^{HUA}_{Mod}		0.2
R^{TIR}_{Obs} versus R^{TIR}_{Mod}		0.34 [0.37]
R^{HUA}_{Obs} versus R^{HUA}_{Mod}		0.32 [0.34]
	R^{TIR}_{Obs}	R^{HUA}_{Obs}
average	70.4 [68.4]	93.7 [89.7]
σ	17.1 [16.6]	24.2 [23.0]
σ/average (%)	24.3 [24.3]	25.8 [25.7]
	R^{TIR}_{Mod}	R^{HUA}_{Mod}
average	57.0	72.0
σ	7.7	11.6
σ/average (%)	13.4	16.1

[a]The superscript i represents the station name ("TIR" for Tirunelveli and "HUA" for Huancayo), and the subscript j represents the type of data ("Obs" for observations and "Mod" for model simulations). The values in square brackets indicate the results obtained using only quiet days (the maximum $Kp \leq 2.0$).

3.3. Equatorial Electrojet

Since the model is shown to reproduce day-to-day $Sq(H)$ variations comparable to observations at ground level, we now examine the source current in the model. Figure 5a shows the average zonal current density at the longitude of Tirunelveli at 0630 UT when this longitude sector is around the noon. See Figure 6 for the height profile of Pedersen and Hall conductivities at Tirunelveli. The results for Huancayo are similar and thus omitted from the figure. The equatorial electrojet is apparent in Figure 5a as a strong eastward current over the magnetic equator at 105 km, in agreement with rocket measurements [*Onwumechili*, 1997]. The peak current density is approximately 5×10^{-6} Am^{-2}. The current density at other latitudes is much smaller (generally less than 20%). The currents are mainly eastward at low latitudes within ±30° magnetic latitudes, and westward currents are dominant at higher altitudes. The maximum westward currents are seen at approximately ±60° magnetic latitudes. The distribution of the zonal current density illustrates the well-known global *Sq* current system with a counterclockwise vortex in the Northern Hemisphere and a clockwise vortex in the Southern Hemisphere [e.g., *Yamazaki et al.*, 2011; *Pedatella et al.*, 2011].

The peak electrojet current density exhibits a significant day-to-day variation, approximately ±25% of the average. Throughout the run, the peak electrojet current is found right on the magnetic equator, which agrees with satellite observations [*Lühr et al.*, 2004]. The variability in the height of the peak electrojet current is also found to be small (±1 km).

Figure 5b shows the ionospheric current system associated with the day-to-day variation of the peak electrojet current, which is extracted using the technique introduced by *MacDougall* [1979a, 1979b]. Briefly, MacDougall's method utilizes the covariance between the variation V_x at a reference point x and the variation V_y at another point y. In our case, V_x is the day-to-day variation of the peak electrojet current, and V_y is the variation at a given height and latitude. Note that V_x and V_y are the variation from the average so that the average of V_x and V_y is zero. It is assumed that V_y is composed of a component that is perfectly correlated with V_x and another component that is noncorrelated with V_x. The former can be described as $c \cdot V_x$, where c is an amplitude factor and the latter is V_z so that $V_y = c \cdot V_x + V_z$. The factor c represents the ratio of the correlated component of current at y to the variable component of peak electrojet current and can be readily obtained by calculating $\mathrm{Cov}(x, y)/\mathrm{Cov}(x, x)$, where Cov denotes the covariance. It may be noted that this method does not examine the cause-and-effect relationship between V_x and V_y, but the results can indicate what physical processes are present. *MacDougall* [1979a, 1979b] applied this method to *Sq* variations at various latitudes in order to determine equivalent current systems associated with the variation in the equatorial electrojet.

The results in Figure 5b reveal that the day-to-day variation of the equatorial electrojet is accompanied by return flow at low and middle magnetic latitudes. (By return flow, we simply mean oppositely directed flow.) The return flow tends to be stronger at lower latitudes, maximizing at the flanks of the electrojet current. This current pattern is consistent with those deduced from *Sq* variations by *MacDougall* [1979a, 1979b]. The formation of the current system in Figure 5b can be interpreted as follows. When variable winds associated with tides and other waves from the lower atmosphere drive electric currents in the dynamo region, they tend to produce a polarization electric field that opposes the currents. For example, if the wind drives a westward perturbation in currents at magnetic low latitudes, then it tends to produce an eastward perturbation in the polarization electric field. The eastward polarization electric field spreads in latitude beyond the generation region and drives an eastward perturbation in the electrojet current at the magnetic

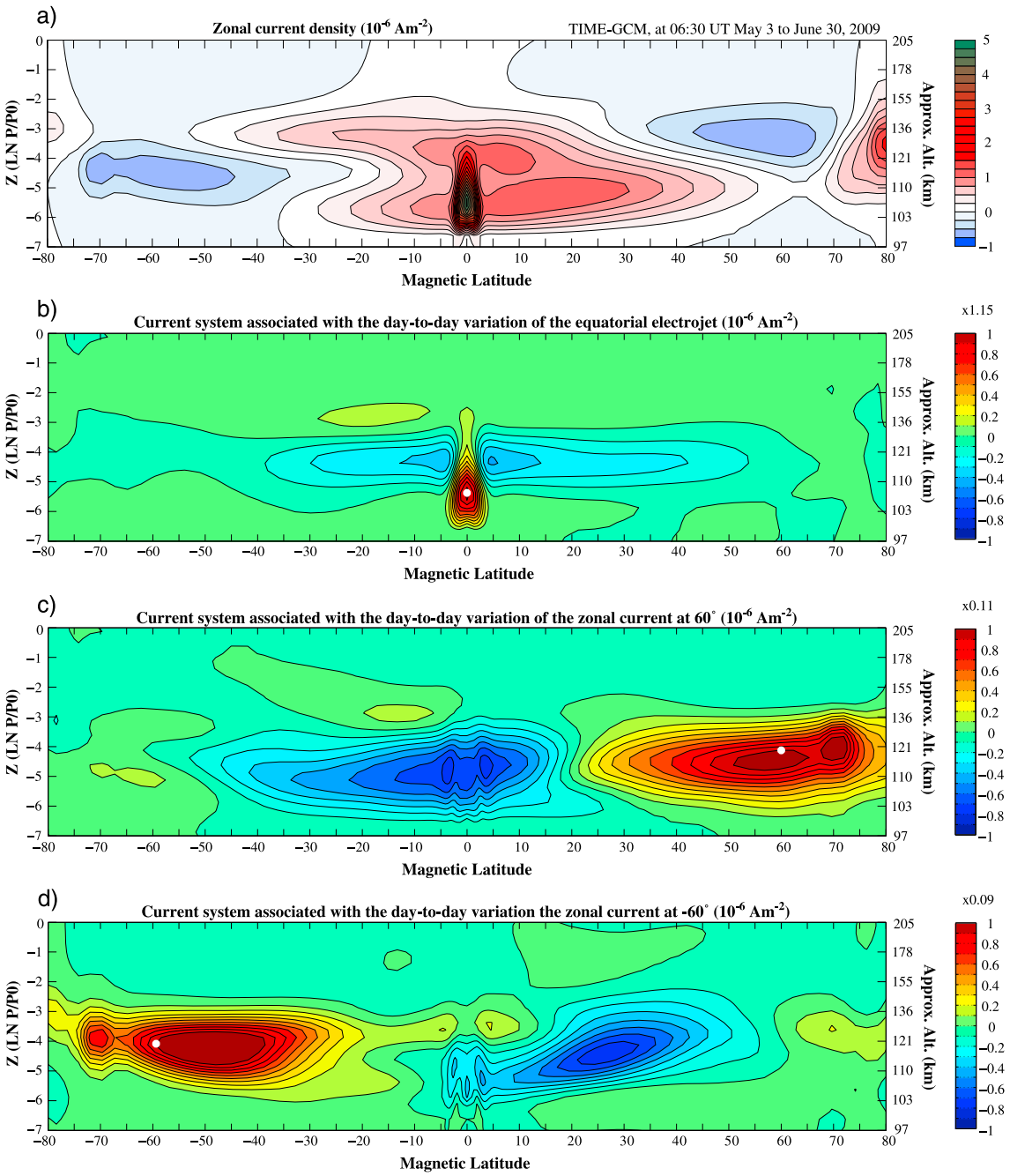

Figure 5. Height versus latitude distributions of the noontime eastward current density at the Indian longitude sector, simulated by the TIME-GCM nudged by the WACCM-X/MERRA/NOGAPS-ALPHA for May and June 2009. (a) The average current density. (b) The current system associated with the day-to-day variation of the peak electrojet current. See the text in section 3.3 for the tracing method. (c) The current system associated with the day-to-day variation of the zonal current at 60° latitude at 120 km. (d) The current system associated with the day-to-day variation of the zonal current at −60° latitude at 120 km. The reference points are indicated by white dots.

equator. Therefore, westward and eastward perturbations in the wind-driven currents at magnetic low latitudes correlate with eastward and westward perturbations in the electrojet current, respectively.

The equatorial electrojet is responsive to perturbations in the zonal electric field because the zonal electric field builds up a vertical polarization electric field, which in turn drives strong zonal Hall currents in the same direction as the zonal electric field. Therefore, paradoxically, eastward and westward wind-driven currents

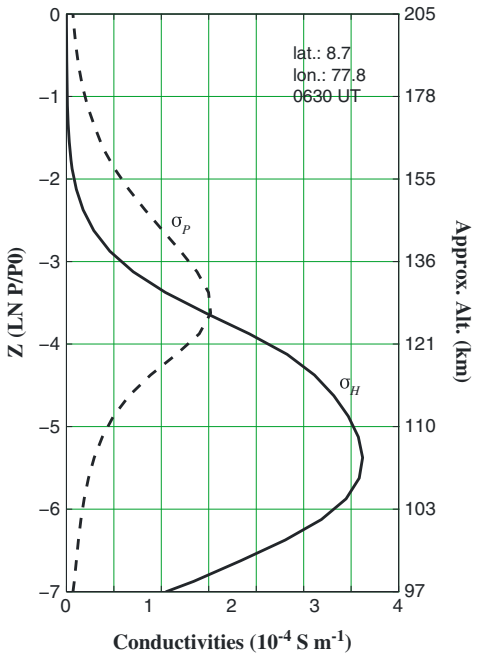

Figure 6. The height profile for the noontime Hall (solid) and Pedersen (dashed) conductivities at Tirunelveli, simulated by the TIME-GCM nudged by the WACCM-X/MERRA/NOGAPS-ALPHA for May and June 2009.

at the magnetic equator can give rise to westward and eastward perturbations in the electrojet current, respectively.

The ionospheric current system in Figure 5b should not be interpreted as the "equatorial electrojet current system." The amount of the electrojet current carried by this current system is less than 25% of the average that is shown in Figure 5a. Therefore, the mechanism mentioned above is valid for the generation of the electrojet variability but does not explain the main component of the equatorial electrojet. The fact that the current pattern in Figure 5b is different from that in Figure 5a indicates that there is a difference between the driving mechanism of the day-to-day variation of the electrojet current, and the generation mechanism of the equatorial electrojet itself. The main driving mechanism of the equatorial electrojet involves global-scale winds in the thermosphere (below 200 km) as the primary source [*Stening*, 1995a; *Du and Stening*, 1999; *Yamazaki et al.*, 2014]. It is also important to note that the dominant mechanism for the electrojet variability can be different on different time scales. Studies of *Sq* variations have shown that changes in the equatorial electrojet intensity and the global-scale *Sq* current system are similar on seasonal or longer time scales [*Stening*, 1995b; *Yamazaki et al.*, 2010], while their variations are generally very different on the shorter time scales [*Osborne*, 1963; *Ogbuehi et al.*, 1967]. It can be inferred that irregular variability in the wind play a dominant role in driving the electrojet variability on a day-to-day time scale, while other mechanisms such as changes in the ionospheric conductivity with solar radiation and zenith angle are also important on a longer time scale.

The ionospheric current system in Figure 5b gives an explanation for a poor correlation between *Sq*(*H*) at the magnetic equator and off the magnetic equator that has been reported by previous researchers [e.g., *Kane*, 1971; *Mann and Schlapp*, 1988]. Our simulation results showed that the correlation coefficient between the daily range of *Sq*(*H*) at the magnetic equator and other latitudes of the same longitude decreases to below 0.5 for a latitudinal separation of 10° (not shown).

MacDougall's method can be used to trace variable currents outside the magnetic equator as well. Figure 5c presents the current system associated with the day-to-day variation of the zonal current at 60° latitude at 120 km, where ionospheric wind dynamo currents are predominantly westward. The region of the positive correlation extends to low latitudes, and the region of the negative correlation extends well into the Southern Hemisphere, illustrating a large-scale current whorl. Figure 5d shows the same but for the southern counterpart, revealing that the variability of the zonal current at −60° also arises from a large-scale current system. These results suggest that the variability of the westward *Sq* currents at ±60° is dominated by large-scale processes, and therefore, the dominant mechanism for the day-to-day variation is probably different for the equatorial electrojet and for the westward *Sq* currents. It is interesting to note that the equatorial enhancement is apparent neither in Figure 5c nor 5d; the reason for which is not clear. Figures 5c and 5d are based on analysis in the longitude sector for Tirunelveli. We found more or less similar results at the longitude sector for Huancayo (not shown). The mechanism for the day-to-day variation of the westward *Sq* currents is to be studied in future work. In this paper, we focus only on the driving mechanism for the electrojet current variability.

3.4. Driving Winds for Electrojet Variability

Day-to-day variations in the noontime peak electrojet current density are compared with day-to-day variations of the neutral wind at various altitudes, latitudes, and longitudes in order to find out where the

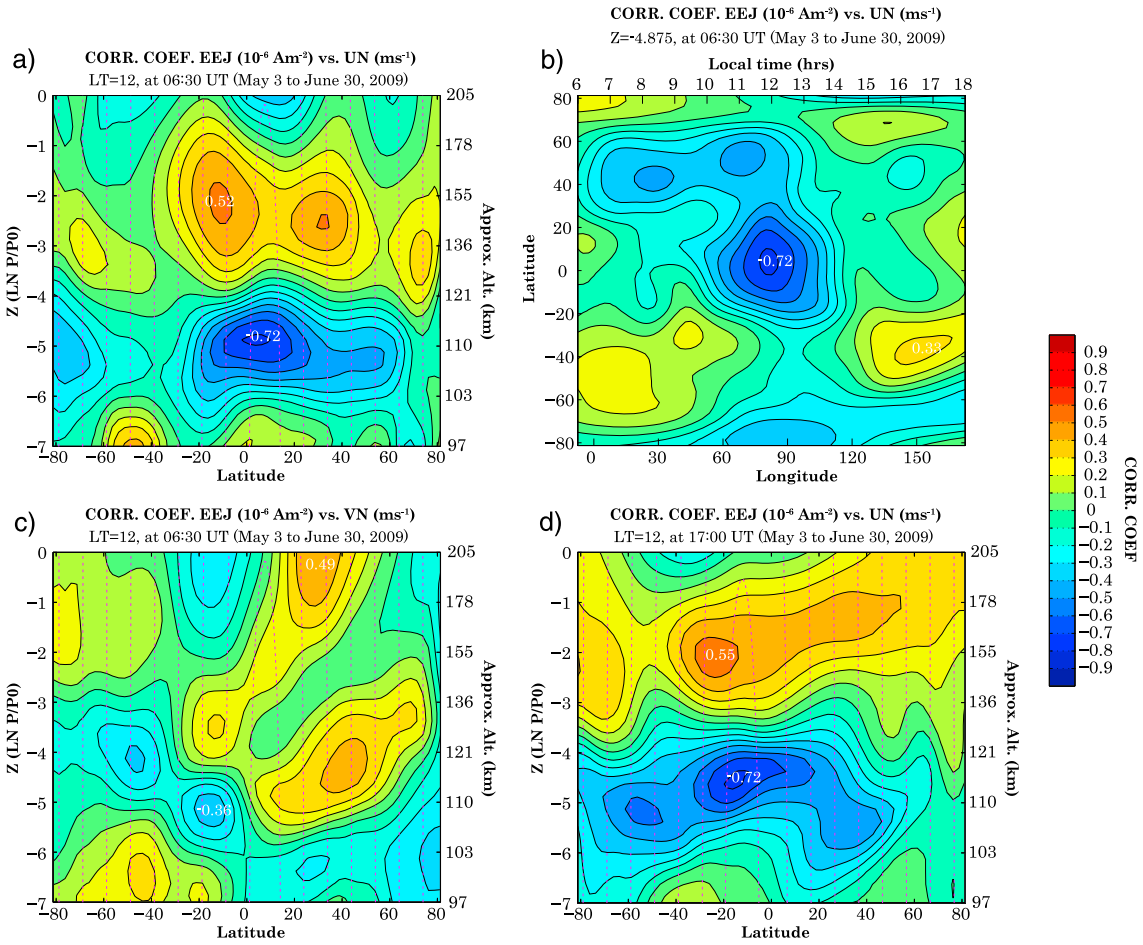

Figure 7. Distributions of the correlation coefficient between the daily peak electrojet current density and (a) the noontime eastward wind at the Indian longitude sector as a function of height and geographic latitude, (b) the eastward wind at ~110 km as a function of geographic latitude and longitude, (c) the noontime northward wind at the Indian longitude sector as a function of height and geographic latitude, and (d) the noontime eastward wind at the Peruvian longitude sector as a function of height and geographic latitude. The magenta dashed lines indicate geomagnetic field lines.

variability of the equatorial electrojet is generated. The correlation coefficient between the peak electrojet current density over Tirunelveli and eastward wind at 0630 UT of each day (noontime for the Indian longitude sector) is plotted in Figure 7a as a function of geographic latitude and height. The negative correlation maximizes over the magnetic equator at approximately 110 km. At this altitude, the wind-driven current is mainly Hall current, which flows in the same direction as the wind. Therefore, an eastward wind perturbation drives an eastward Hall current, which in turn produces a westward polarization electric field that reduces the eastward electrojet current at the magnetic equator, as we discussed in section 3.3. On the other hand, at 150 km, where the Pedersen conductivity is larger than the Hall conductivity, an eastward wind perturbation drives a poleward current and an equatorward polarization electric field. The polarization electric field is transmitted down to the Hall region along equipotential magnetic field lines, where it drives a westward Hall current and an eastward polarization electric field that reinforces the eastward electrojet current. As a result, the eastward wind is negatively and positively correlated with the eastward equatorial electrojet current in the Hall and Pedersen regions, respectively. The correlation is more significant in the Hall region as the wind variability due to lower atmospheric forcing is more significant at 110 km than at 150 km, and thus produces more variability in the equatorial electrojet.

Figure 7b shows the correlation coefficient as a function of geographic latitude and longitude at ~110 km. The correlation is rapidly lost with increasing distance from the magnetic equator and the noontime longitude sector (i.e., 82.5° longitude). Figure 7c is the same as Figure 7a but for the northward wind. Overall, the correlation is small, indicating that the variability in the meridional wind makes little contribution to the

day-to-day variation of the equatorial electrojet. Previously, *Du and Stening* [1999] showed that the meridional component of the global wind drives more electrojet currents than the zonal component does. This, again, highlights the difference between the driving mechanism of the day-to-day variation of the electrojet current, and the generation mechanism of the equatorial electrojet itself.

Figure 7d shows the results for the Peruvian longitude sector. The results are similar with those for the Indian longitude sector in Figure 7a, but the region of the maximum negative correlation is in the Southern Hemisphere, as is the magnetic equator. This confirms that the winds that are important for the day-to-day variation of the equatorial electrojet are those over the magnetic equator, not the geographic equator.

Since we have shown a good correlation between the noontime peak electrojet current density and the noontime zonal wind at ~110 km near the magnetic equator, one may wonder what causes the day-to-day variability in the noontime zonal wind. Figure 2 depicts variations in the hourly zonal wind speed at 110 km over Tirunelveli and Huancayo. If we pick up the data corresponding to the local noon at each station and compare them with the corresponding noontime peak electrojet current density, the correlation coefficient is about 0.7 at both stations, as shown in Figure 7. At each station, we computed the diurnal and semidiurnal amplitudes and time mean in the zonal wind for each 24 h period starting from the local midnight and compared them with the noontime zonal wind. At Tirunelveli, the day-to-day variation in the noontime zonal wind is positively and negatively correlated with the diurnal and semidiurnal tidal amplitudes, respectively ($r = 0.41$ and $r = -0.40$). The correlation between the noontime zonal wind and mean wind is found to be small (r =0.05). On the other hand, at Huancayo, the day-to-day variation in the noontime wind is correlated with the mean wind (r =0.51) but uncorrelated with the diurnal and semidiurnal amplitudes ($r = 0.05$ and $r = -0.08$, respectively). Therefore, the day-to-day variations in the tidal waves are important at Tirunelveli, while the mean wind is important at Huancayo for this period. This seems to indicate that irregular variability in the wind is ubiquitous, but the cause of the variability can be different for different geographical locations and perhaps for different periods.

4. Conclusions

We have examined day-to-day variations of the equatorial electrojet reproduced by the TIME-GCM. The lower part of the TIME-GCM (below 95 km) was constrained by the WACCM-X/MERRA/NOGAPS-ALPHA in order to incorporate variable tidal waves and other large-scale atmospheric waves in the lower atmosphere. Those waves propagate to higher levels and provide irregular variability in the neutral wind at dynamo region heights where ionospheric currents are driven by the neutral wind. The model was run with constant solar and magnetospheric energy inputs so that the ionospheric variability is generated solely by the lower atmospheric forcing. The following are the main results of the simulation:

1. The peak electrojet current density changes from day to day (±25% of the average) due to irregular variability of the neutral wind, which in turn produces day-to-day variations in the daily range of $Sq(H)$ near the magnetic equator (±15% of the average). The variability in the height and latitude of the peak electrojet current is small.
2. The ionospheric current system associated with the day-to-day variation of the electrojet current shows return flow at low and middle magnetic latitudes with its maxima at the flanks of the electrojet current. This results in a poor correlation between $Sq(H)$ at the magnetic equator and off the magnetic equator that has been reported by earlier researchers.
3. The day-to-day variation in the noontime eastward electrojet current correlates with the westward wind at 100–120 km altitudes near the magnetic equator. The meridional wind is not effective in driving day-to-day variability of the equatorial electrojet.

Previous studies that used models of the equatorial electrojet with assumed zonal electric fields and zonal winds [e.g., *Richmond*, 1973; *Reddy and Devasia*, 1981; *Stening*, 1985; *Anandarao and Raghavarao*, 1987; *Hysell et al.*, 2002] found that the wind affects the meridional polarization electric field and the zonal current, but these studies were unable to calculate the response of the zonal polarization electric field to the zonal winds. *Fang et al.* [2008b], using a model with self-consistent electrodynamics, showed evidence that winds at low and middle latitudes can alter the zonal polarization field to affect the electrojet. The present study has shown how the response of the zonal polarization electric field to the zonal wind is the main source of the day-to-day variation of the equatorial electrojet.

Acknowledgments
We thank Qian Wu for his comments on a draft of this paper. The solar activity index $F_{10.7}$ was provided by the Herzberg Institute of Astrophysics. Geomagnetic indicies *Kp* and *Dst* were provided by World Data Center for Geomagnetism, Kyoto. The numerical data from the simulation will be made available upon request. Y.Y. was supported by a research fellowship of the Japan Society for the Promotion of Science (JSPS) for research abroad. A.R., A.M., and H.L. were supported in part by NASA grant NNX09AN57G and NSF grant AGS1138784. A.R. and H.L. were also supported by NASA grant NNX09AJ83G. A.M. was also supported by NASA grant NNX13AF77G. F.S. and H.L. were partially supported by NASA/LWS grant NNH12AT21L. In addition, F.S. was also supported by ONR 6.1 base funding. WACCM-X simulations were supported by a grant of computer time from the DoD High Performance Computing Modernization Program at the U.S. Navy DoD Supercomputing Resource Center (NAVO). The National Center for Atmospheric Research is sponsored by the National Science Foundation.

Alan Rodger thanks the reviewers for their assistance in evaluating this paper.

References

Alken, P., and S. Maus (2007), Spatio-temporal characterization of the equatorial electrojet from CHAMP, Ørsted, and SAC-C satellite magnetic measurements, *J. Geophys. Res.*, *112*, A09305, doi:10.1029/2007JA012524.

Anandarao, B. G., and R. Raghavarao (1987), Structural changes in the currents and fields of the equatorial electrojet due to zonal and meridional winds, *J. Geophys. Res.*, *92*(A3), 2514–2526, doi:10.1029/JA092iA03p02514.

Briggs, B. H. (1984), The variability of ionospheric dynamo currents, *J. Atmos. Terr. Phys.*, *59*, 497–509.

Blanc, M., and A. Richmond (1980), The ionospheric disturbance dynamo, *J. Geophys. Res.*, *85*(A4), 1669–1686, doi:10.1029/JA085iA04p01669.

Campbell, W. H. (2003), *Introduction to Geomagnetic Fields,* 2nd ed., Cambridge Univ. Press, Cambridge, U. K.

Chapman, S., and J. Bartels (1940), *Geomagnetism*, Oxford Univ. Press, London, U. K.

Chang, L. C., S. E. Palo, and H.-L. Liu (2011), Short-term variability in the migrating diurnal tide caused by interactions with the quasi 2 day wave, *J. Geophys. Res.*, *116*, D12112, doi:10.1029/2010JD014996.

Davis, R. N., J. Du, A. K. Smith, W. E. Ward, and N. J. Mitchell (2013), The diurnal and semidiurnal tides over Ascension Island (8°S, 14°W) and their interaction with the stratospheric QBO: Studies with meteor radar, eCMAM and WACCM, *Atmos. Chem. Phys. Discuss.*, *13*, 4785–4837, doi:10.5194/acpd-13-4785-2013.

Eckermann, S. D., K. W. Hoppel, L. Coy, J. P. McCormack, D. E. Siskind, K. Nielsen, A. Kochenash, M. H. Stevens, C. R. Englert, and M. Hervig (2009), High-altitude data assimilation system experiments for the northern summer mesosphere season of 2007, *J. Atmos. Sol. Terr. Phys.*, *71*, 531–551.

Du, J., and R. J. Stening (1999), Simulating the ionospheric dynamo. II. Equatorial electric fields, *J. Atmos. Sol. Terr. Phys.*, *61*, 925–940.

Fang, T.-W., A. D. Richmond, J. Y. Liu, A. Maute, C. H. Lin, C. H. Chen, and B. Harper (2008a), Model simulation of the equatorial electrojet in the Peruvian and Philippine sectors, *J. Atmos. Sol. Terr. Phys.*, *70*, 2203–2211, doi:10.1016/j.jastp.2008.04.021.

Fang, T.-W., A. D. Richmond, J. Y. Liu, and A. Maute (2008b), Wind dynamo effects on ground magnetic perturbations and vertical drifts, *J. Geophys. Res.*, *113*, A11313, doi:10.1029/2008JA013513.

Fang, T.-W., R. Akmaev, T. Fuller-Rowell, F. Wu, N. Maruyama, and G. Millward (2013), Longitudinal and day-to-day variability in the ionosphere from lower atmosphere tidal forcing, *Geophys. Res. Lett.*, *40*, 2523–2528, doi:10.1002/grl.50550.

Finlay, C. C., et al. (2010), International geomagnetic reference field: The eleventh generation, *Geophys. J. Int.*, *183*, 1216–1230, doi:10.1111/j.1365-246X.2010.04804.x.

Forbes, J. M. (1981), The equatorial electrojet, *Rev. Geophys.*, *19*(3), 469–504, doi:10.1029/RG019i003p00469.

Forbes, J. M., and X. Zhang (2012), Lunar tide amplification during the January 2009 stratosphere warming event: Observations and theory, *J. Geophys. Res.*, *117*, A12312, doi:10.1029/2012JA017963.

Forbes, J. M., X. Zhang, S. Bruinsma, and J. Oberheide (2013), Lunar semidiurnal tide in the thermosphere under solar minimum conditions, *J. Geophys. Res. Space Physics*, *118*, 1788–1801, doi:10.1029/2012JA017962.

Gagnepain, J., M. Crochet, and A. D. Richmond (1977), Comparison of equatorial electrojet models, *J. Atmos. Terr. Phys.*, *39*, 1119–1124.

Gurubaran, S. (2002), The equatorial counter electrojet: Part of a worldwide current system?, *Geophys. Res. Lett.*, *29*(9), 1337, doi:10.1029/2001GL014519.

Hagan, M. E., R. G. Roble, and J. Hackney (2001), Migrating thermospheric tides, *J. Geophys. Res.*, *106*, 12,739–12,752, doi:10.1029/2000JA000344.

Hasegawa, M. (1960), On the position of the focus of the geomagnetic Sq current system, *J. Geophys. Res.*, *65*(5), 1437–1447, doi:10.1029/JZ065i005p01437.

Hoppel, K. W., N. L. Baker, L. Coy, S. D. Eckermann, J. P. McCormack, G. Nedoluha, and D. E. Siskind (2008), Assimilation of stratospheric and mesospheric temperatures from MLS and SABER in a global NWP model, *Atmos. Chem. Phys. Discuss.*, *8*, 8455–8490.

Huang, C.-M., A. D. Richmond, and M.-Q. Chen (2005), Theoretical effects of geomagnetic activity on low-latitude ionospheric electric fields, *J. Geophys. Res.*, *110*, A05312, doi:10.1029/2004JA010994.

Hysell, D. L., J. L. Chau, and C. G. Fesen (2002), Effects of large horizontal winds on the equatorial electrojet, *J. Geophys. Res.*, *107*(A8), SIA 27-1–SIA 27-12, doi:10.1029/2001JA000217.

Jin, H., Y. Miyoshi, H. Fujiwara, H. Shinagawa, K. Terada, N. Terada, M. Ishii, Y. Otsuka, and A. Saito (2011), Vertical connection from the tropospheric activities to the ionospheric longitudinal structure simulated by a new Earth's whole atmosphere-ionosphere coupled model, *J. Geophys. Res.*, *116*, A01316, doi:10.1029/2010JA015925.

Kane, R. P. (1971), Relationship between H ranges at equatorial and middle latitudes, *J. Atmos. Terr. Phys.*, *33*, 319–327.

Kawano-Sasaki, K., and S. Miyahara (2008), A study on three-dimensional structures of the ionospheric dynamo currents induced by the neutral winds simulated by the Kyushu-GCM, *J. Atmos. Sol. Terr. Phys.*, *70*, 1549–1562.

Khattatov, B. V., M. A. Geller, V. A. Yubin, and P. B. Hays (1997), Diurnal migrating tide as seen by the high-resolution Doppler imager/UARS: 2. Monthly mean global zonal and vertical velocities, pressure, temperature, and inferred dissipation, *J. Geophys. Res.*, *102*(D4), 4423–4435, doi:10.1029/96JD03654.

Kikuchi, T., K. K. Hashimoto, and K. Nozaki (2008), Penetration of magnetospheric electric fields to the equator during a geomagnetic storm, *J. Geophys. Res.*, *113*, A06214, doi:10.1029/2007JA012628.

Le Huy, M., and C. Amory-Mazaudier (2005), Magnetic signature of the ionospheric disturbance dynamo at equatorial latitudes: "D_{dyn}", *J. Geophys. Res.*, *110*, A10301, doi:10.1029/2004JA010578.

Liu, H.-L. (2014), WACCM-X simulation of tidal and planetary wave variability in the upper atmosphere, in *Modeling the Ionosphere-Thermosphere System,* edited by J. Huba, R. Schunk, and G. Khazanov, John Wiley, Chichester, U. K., doi:10.1002/9781118704417.ch16.

Liu, H.-L., et al. (2010a), Thermosphere extension of the whole atmosphere community climate model, *J. Geophys. Res.*, *115*, A12302, doi:10.1029/2010JA015586.

Liu, H.-L., W. Wang, A. D. Richmond, and R. G. Roble (2010b), Ionospheric variability due to planetary waves and tides for solar minimum conditions, *J. Geophys. Res.*, *115*, A00G01, doi:10.1029/2009JA015188.

Liu, H.-L., V. A. Yudin, and R. G. Roble (2013), Day-to-day ionospheric variability due to lower atmosphere perturbations, *Geophys. Res. Lett.*, *40*, 665–670, doi:10.1002/grl.50125.

Lühr, H., and C. Manoj (2013), The complete spectrum of the equatorial electrojet related to solar tides: CHAMP observations, *Ann. Geophys.*, *31*, 1315–1331, doi:10.5194/angeo-31-1315-2013.

Lühr, H., S. Maus, and M. Rother (2004), Noon-time equatorial electrojet: Its spatial features as determined by the CHAMP satellite, *J. Geophys. Res.*, *109*, A01306, doi:10.1029/2002JA009656.

MacDougall, J. W. (1979a), Equatorial electrojet and Sq current system—Part I, *J. Geomagn. Geoelectr.*, *31*, 341–357.

MacDougall, J. W. (1979b), Equatorial electrojet and Sq current system—Part II, *J. Geomagn. Geoelectr.*, *31*, 359–372.
Mann, R. J., and D. M. Schlapp (1988), The equatorial electrojet and the day-to-day variability of Sq, *J. Atmos. Terr. Phys.*, *30*, 1761–1776.
Marsal, S., A. D. Richmond, A. Maute, and B. J. Anderson (2012), Forcing the TIEGCM model with Birkeland currents from the active magnetosphere and planetary electrodynamics response experiment, *J. Geophys. Res.*, *117*, A06308, doi:10.1029/2011JA017416.
Matsushita, S. (1967), Solar quiet and lunar daily variation fields, in *Physics of Geomagnetic Phenomena*, edited by S. Matsushita and W. H. Campbell, pp. 301–424, Academic Press, New York.
Miyahara, S. (1978), Zonal mean wind induced by vertically propagating atmospheric tidal waves in the lower thermosphere, *J. Meteorol. Soc. Jpn.*, *56*, 86–97.
Miyahara, S., and J. M. Forbes (1991), Interaction between gravity waves and the diurnal tide in the mesosphere and lower thermosphere, *J. Meteorol. Soc. Jpn.*, *69*, 523–531.
Miyahara, S., and M. Ooishi (1997), Variation of Sq induced by atmospheric tides simulated by a middle atmosphere general circulation model, *J. Geomagn. Geoelectr.*, *49*, 77–87.
Ogbuehi, P. O., A. Onwumechilli, and S. O. Ifedili (1967), The equatorial electrojet and world-wide Sq currents, *J. Atmos. Terr. Phys.*, *29*, 149–160.
Onwumechili, C. A. (1997), *The Equatorial Electrojet*, CRC Press, Boca Raton, Fla.
Osborne, D. G. (1963), Daily variability in strength of equatorial electrojet, *J. Geophys. Res.*, *68*, 2435–2439.
Pedatella, N. M., J. M. Forbes, and A. D. Richmond (2011), Seasonal and longitudinal variations of the solar quiet (Sq) current system during solar minimum determined by CHAMP satellite magnetic field observations, *J. Geophys. Res.*, *116*, A04317, doi:10.1029/2010JA016289.
Pedatella, N. M., H.-L. Liu, A. D. Richmond, A. Maute, and T.-W. Fang (2012), Simulations of solar and lunar tidal variability in the mesosphere and lower thermosphere during sudden stratosphere warmings and their influence on the low-latitude ionosphere, *J. Geophys. Res.*, *117*, A08326, doi:10.1029/2012JA017858.
Pedatella, N. M., et al. (2014a), The neutral dynamics during the 2009 sudden stratosphere warming simulated by different whole atmosphere models, *J. Geophys. Res. Space Physics*, *119*, 1306–1324, doi:10.1002/2013JA019421.
Pedatella, N. M., H.-L. Liu, F. Sassi, J. Lei, J. L. Chau, and X. Zhang (2014b), Ionosphere variability during the 2009 SSW: Influence of the lunar semidiurnal tide and mechanisms producing electron density variability, *J. Geophys. Res. Space Physics*, *119*, 3828–3843, doi:10.1002/2014JA019849.
Rastogi, R. G. (1974), Lunar effects in the counter electrojet near the magnetic equator, *J. Atmos. Terr. Phys.*, *36*, 167–170.
Rastogi, R. G. (1989), The equatorial electrojet, in *Geomagnetism*, vol. 3, edited by J. Jacobs, pp. 461–525, Academic Press, San Diego, Calif.
Rastogi, R. G., and N. B. Trivedi (1970), Luni-solar tides in H at stations within the equatorial electrojet, *Planet. Space Sci.*, *18*(3), 367–377.
Reddy, C. A., and C. V. Devasia (1981), Height and latitude structure of electric fields and currents due to local east-west winds in the equatorial electrojet, *J. Geophys. Res.*, *86*, 5751–5767.
Richards, P. G., J. A. Fennelly, and D. G. Torr (1994), EUVAC: A solar EUV flux model for aeronomic calculations, *J. Geophys. Res.*, *99*(A5), 8981–8992, doi:10.1029/94JA00518.
Richmond, A. D. (1973), Equatorial electrojet—I. Development of a model including winds and instabilities, *J. Atmos. Terr. Phys.*, *35*, 1083–1103.
Richmond, A. D. (1995a), The ionospheric wind dynamo: Effects of its coupling with different atmospheric regions, in *The Upper Mesosphere and Lower Thermosphere: A Review of Experiment and Theory, Geophys. Monogr. Ser.*, vol. 87, edited by R. M. Johnson and T. L. Killeen, pp. 49–65, AGU, Washington, D. C, doi:10.1029/GM087p0049.
Richmond, A. D. (1995b), Ionospheric electrodynamics using magnetic apex coordinates, *J. Geomagn. Geoelectr.*, *47*, 191–212.
Richmond, A. D., and A. Maute (2014), Ionospheric electrodynamics modeling, in *Modeling the Ionosphere-Thermosphere System*, edited by J. Huba, R. Schunk, and G. Khazanov, John Wiley, Chichester, U. K., doi:10.1002/9781118704417.ch6.
Richmond, A. D., and R. G. Roble (1987), Electrodynamic effects of thermospheric winds from the NCAR thermospheric general circulation model, *J. Geophys. Res.*, *92*(A11), 12,365–12,376, doi:10.1029/JA092iA11p12365.
Richmond, A. D., S. Matsushita, and J. D. Tarpley (1976), On the production mechanism of electric currents and fields in the ionosphere, *J. Geophys. Res.*, *81*(4), 547–555, doi:10.1029/JA081i004p00547.
Richmond, A. D., E. C. Ridley, and R. G. Roble (1992), A thermosphere/ionosphere general circulation model with coupled electrodynamics, *Geophys. Res. Lett.*, *19*, 601–604, doi:10.1029/92GL00401.
Rienecker, M. M., et al. (2011), MERRA—NASA's Modern-Era Retrospective Analysis for research and applications, *J. Clim.*, *24*, 3624–3648, doi:10.1175/JCLI-D-11-00015.1.
Roble, R. G., and E. C. Ridley (1994), A thermosphere-ionosphere-mesosphere-electrodynamics general circulation model (TIME-GCM): Equinox solar cycle minimum simulations (30–500 km), *Geophys. Res. Lett.*, *21*, 417–420.
Sassi, F., H.-L. Liu, J. Ma, and R. R. Garcia (2013), The lower thermosphere during the Northern Hemisphere winter of 2009: A modeling study using high-altitude data assimilation products in WACCM-X, *J. Geophys. Res. Atmos.*, *118*, 8954–8968, doi:10.1002/jgrd.50632.
Schlapp, D. M. (1968), World-wide morphology of day-to-day variability of Sq, *J. Atmos. Terr. Phys.*, *30*, 1761–1776.
Shinbori, A., et al. (2010), Anomalous occurrence features of the preliminary impulse of geomagnetic sudden commencement in the South Atlantic Anomaly region, *J. Geophys. Res.*, *115*, A08309, doi:10.1029/2009JA015035.
Stening, R. J. (1977), Magnetic variations at other latitudes during reverse equatorial electrojet, *J. Atmos. Terr. Phys.*, *39*, 1071–1077, doi:10.1016/0021-9169(77)90015-0.
Stening, R. J. (1985), Modeling the equatorial electrojet, *J. Geophys. Res.*, *90*(A2), 1705–1719, doi:10.1029/JA090iA02p01705.
Stening, R. J. (1995a), What drives the equatorial electrojet?, *J. Atmos. Terr. Phys.*, *57*, 1117–1128.
Stening, R. J. (1995b), Variations in the strength of the Sq current system, *Ann. Geophys.*, *13*, 627–632.
Stening, R. J. (2003), Space weather in the equatorial ionosphere, *Space Sci. Rev.*, *107*, 263–271.
Stening, R. J., J. M. Forbes, M. E. Hagan, and A. D. Richmond (1997), Experiments with a lunar atmospheric tidal model, *J. Geophys. Res.*, *102*(D12), 13,465–13,471, doi:10.1029/97JD00778.
Takeda, M. (1984), Day-to-day variation of equivalent Sq current system during March 11–26, 1970, *J. Geomagn. Geoelectr.*, *36*, 215–228.
Teitelbaum, H., and F. Vial (1991), On tidal variability induced by nonlinear interaction with planetary waves, *J. Geophys. Res.*, *96*(A8), 14,169–14,178, doi:10.1029/91JA01019.
Teitelbaum, H., F. Vial, A. H. Manson, R. Giraldez, and M. Massebeuf (1989), Non-linear interaction between the diurnal and semidiurnal tides: Terdiurnal and diurnal secondary waves, *J. Atmos. Terr. Phys.*, *51*, 627–634.
Wu, Q., T. L. Killeen, D. A. Ortland, S. C. Solomon, R. D. Gablehouse, R. M. Johnson, W. R. Skinner, R. J. Niciejewski, and S. J. Franke (2006), TIMED Doppler interferometer (TIDI) observations of migrating diurnal and semidiurnal tides, *J. Atmos. Sol. Terr. Phys.*, *68*, 408–417.

Wu, Q., D. A. Ortland, T. L. Killeen, R. G. Roble, M. E. Hagan, H.-L. Liu, S. C. Solomon, J. Xu, W. R. Skinner, and R. J. Niciejewski (2008), Global distribution and interannual variations of mesospheric and lower thermospheric neutral wind diurnal tide: 1. Migrating tide, *J. Geophys. Res.*, *113*, A05308, doi:10.1029/2007JA012542.

Xu, J., A. K. Smith, H.-L. Liu, W. Yuan, Q. Wu, G. Jiang, M. G. Mlynczak, J. M. Russell III, and S. J. Franke (2009), Seasonal and quasi-biennial variations in the migrating diurnal tide observed by thermosphere, ionosphere, mesosphere, energetics and dynamics (TIMED), *J. Geophys. Res.*, *114*, D13107, doi:10.1029/2008JD011298.

Yamazaki, Y., and A. D. Richmond (2013), A theory of ionospheric response to upward-propagating tides: Electrodynamic effects and tidal mixing effects, *J. Geophys. Res. Space Physics*, *118*, 5891–5905, doi:10.1002/jgra.50487.

Yamazaki, Y., K. Yumoto, T. Uozumi, S. Abe, M. G. Cardinal, D. McNamara, R. Marshall, B. M. Shevtsov, and S. I. Solovyev (2010), Reexamination of the Sq-EEJ relationship based on extended magnetometer networks in the east Asian region, *J. Geophys. Res.*, *115*, A09319, doi:10.1029/2010JA015339.

Yamazaki, Y., et al. (2011), An empirical model of the quiet daily geomagnetic field variation, *J. Geophys. Res.*, *116*, A10312, doi:10.1029/2011JA016487.

Yamazaki, Y., K. Yumoto, D. McNamara, T. Hirooka, T. Uozumi, K. Kitamura, S. Abe, and A. Ikeda (2012), Ionospheric current system during sudden stratospheric warming events, *J. Geophys. Res.*, *117*, A03334, doi:10.1029/2011JA017453.

Yamazaki, Y., A. D. Richmond, A. Maute, Q. Wu, D. A. Ortland, A. Yoshikawa, I. A. Adimula, B. Rabiu, M. Kunitake, and T. Tsugawa (2014), Ground magnetic effects of the equatorial electrojet simulated by the TIE-GCM driven by TIMED satellite data, *J. Geophys. Res. Space Physics*, *119*, 3150–3161, doi:10.1002/2013JA019487.

Zhang, J. T., and J. M. Forbes (2013), Lunar tidal winds between 80 and 110 km from UARS/HRDI wind measurements, *J. Geophys. Res. Space Physics*, *118*, 5296–5304, doi:10.1002/jgra.50420.